

Electron self-energy corrections using the Welton concept for atomic structure calculations

T.V.B. Nguyen^a, J.A. Lowe^a, T.L.H. Pham^a, I.P. Grant^b, C.T. Chantler^{a,*}

^a School of Physics, The University of Melbourne, Australia

^b Mathematical Institute, Oxford University, Oxford, UK

ARTICLE INFO

Keywords:

Self energy
Hydrogenic screening
Atomic structure
QED

ABSTRACT

The high level of accuracy achieved by atomic experiments in recent time has shone a spotlight on the need for a similarly high level of accuracy in atomic structure calculations, and in particular, QED prediction. A method of electron self-energy correction originally derived from the Welton idea by Lowe et al. (2013) (LCG-Welton method) has now been fully incorporated into the popular atomic structural package, GRASP2K, which we have introduced in this paper. A series of benchmark tests and results are presented, which enables the comparison of the implementations of different versions of GRASP2K, and the implementations on different platforms or operating systems. Test results presented in this paper demonstrate that these new implementations maintain the overall consistency and stability of the program across various platforms, while at the same time improve the accuracy of final energies. Our calculations for hydrogenic $Ly_{\alpha_{1,2}}$ transitions show excellent agreement with experiment, to within less than 0.5 eV. On helium-like systems, our calculations show an improvement from the previous GRASP2K screening method. The new results from electronic self-energy contribution using the LCG-Welton method is more consistent with current standards in the literature, where they now fit within experimental variability of up to 0.1 eV. An option for users to adjust the gauge factor in the electric component of the transition rate has also been added to facilitate further investigation of this particular topic.

1. Introduction

We present a revised version of the relativistic configuration interaction (RCI) program belonging to the GRASP2K v1.1 developed by Jönsson et al. (2013). The changes relate particularly to the RCI program, which is now called RCI4. A self-energy screening method based on Welton's idea is made the default technique of calculation. Whilst many other qualitatively different implementations of the Welton idea have been made in the literature, and there have been relativistic implementations (Indelicato and Mohr, 2001), this is the first implementation in a GRASP2K version and is a new approach. Non-default options are available for users to select other methods of calculation, including the original GRASP screening method.

Self-energy screening following the concept introduced by Welton (1948) was investigated in the GRASP2K v1.0 codes (Lowe et al., 2013). In that work, a patch was prepared to permit use of the latest available hydrogenic values, together with modifications to account for finite-nuclear-size effects. The results of this implementation of Welton's idea show remarkable agreement with the latest advanced full QED calculations for helium-like and many-electron systems (Lowe et al., 2013), such as those of Artemyev et al. (2005) and Indelicato and Mohr (2001).

2. Self-energy approximation in many-electron atoms

The major change of this revision has been to develop and implement the LCG-Welton (Lowe–Chantler–Grant–Welton) approach for the electron self-energy (Lowe et al., 2013) within the GRASP2K v1.1 package. Further, this updates the self-energy calculations to use the latest available hydrogenic values (Mohr and Kim, 1992; Indelicato et al., 1998; Le Bigot et al., 2001) and also accounts for finite-nuclear-size effects. The Welton idea can be used in a variety of forms, with very different predictions of QED self-energy expectation values and shielding. If we consider an electron moving in a potential $V(\mathbf{x})$, with its motion due to fluctuations in the electromagnetic field as $\Delta\mathbf{x}$, then the mean-square radius of oscillation is

$$\langle(\Delta\mathbf{x})^2\rangle = \frac{2}{\pi} \frac{e^2}{\hbar c} \left(\frac{\hbar^2}{mc}\right) \int_{k_0}^k \frac{dk}{k}, \quad (1)$$

which diverges at both the upper and lower limit. The divergence at the lower limit disappears for an electron in any sort of finite nuclear potential, or with a finite low-frequency cut-off, whilst the upper limit

* Corresponding author.

E-mail address: chantler@unimelb.edu.au (C.T. Chantler).

is truncated at $k = mc/\hbar$. Then the integrals are suitably finite. We can expand the instantaneous potential energy as

$$V(\mathbf{x} + \Delta\mathbf{x}) = \left[1 + (\Delta\mathbf{x} \cdot \nabla) + \frac{1}{2}(\Delta\mathbf{x} \cdot \nabla)^2 + \dots \right] V(\mathbf{x}). \quad (2)$$

For the average, odd orders cancel and the average potential energy from three orthogonal axes is then

$$\langle V(\mathbf{x} + \Delta\mathbf{x}) \rangle = \left[1 + \frac{1}{6} \langle (\Delta\mathbf{x})^2 \rangle \nabla^2 + \dots \right] V(\mathbf{x}). \quad (3)$$

Elaborate QED calculations of the lowest order contribution to the self-energy of a bound electron in the field of static point nuclei and finite nuclei have been carried out by Mohr (1974) and others, and are comprehensively tabulated for lower principal quantum numbers, n . In many-electron atoms, an orbital electron moves in the potential of a finite distribution of nuclear charge modified by the potential of atomic electrons and other effects. In the Welton idea, the contribution to the potential energy from the perturbed motion of a single electron wave function ψ is proportional to $\nabla^2 V(\mathbf{x})$,

$$E_{SE} \approx \frac{1}{6} \int \psi^\dagger(\mathbf{x}) (\Delta\mathbf{x})^2 \cdot \nabla^2 V(\mathbf{x}) \cdot \psi(\mathbf{x}) d^3\mathbf{x}, \quad (4)$$

which suggests modelling the self-energy in the many-electron atom (Lowe et al., 2013) as

$$E_{SE} = \frac{\langle \phi | \nabla^2 V(\mathbf{x}) | \phi \rangle}{\langle \psi^H | \nabla^2 V(\mathbf{x}) | \psi^H \rangle} E_{SE}^H. \quad (5)$$

The vacuum polarisation and self-energy (SE) screening methods listed (Lowe et al., 2013) for a single orbital are retained in this version. In a many-electron atom, the wave function for each atomic state (an Atomic State Function, ASF) is

$$\Psi_{\Gamma} = \sum_{\gamma} C_{\Gamma,\gamma} \Phi_{\gamma} \quad (6)$$

where Φ_{γ} are a set of N -electron configuration state functions (CSFs) represented by the quantum labels γ , including a total angular momentum J and parity P . Each CSF is an antisymmetrised product of Dirac orbitals ϕ_i . If the generalised occupation number of the orbital i in the CSF is $\tilde{N}_{\gamma,i}$ in Φ_{γ} , then this contributes

$$E_{SE}^j(\gamma) = \sum_i \tilde{N}_{\gamma,i} E_{SE,i}^j, \quad (7)$$

where j is the choice of approximation from the list below. Assuming no off-diagonal CSF contributions, the total ASF self-energy is

$$E_{SE}^{\Gamma, \text{total, ASF}} = \sum_{\gamma} C_{\Gamma,\gamma}^2 E_{SE}^j(\gamma) \quad (8)$$

For a single unexpanded CSF, with no correlation orbitals, occupation numbers are generally unity or zero (occupied or unoccupied), as in the example and comparison above. However, GRASP2K permits expansion into correlation orbitals to improve convergence of the wavefunction but with potentially different symmetries, numbers of nodes, and limits.

Should correlation orbitals be included in the sum, or excluded? Spectroscopic orbitals dominate the computation of physical observables. The correlated orbitals are there to improve the wave function and are not so constrained, so it might be queried as to whether the Welton idea can or should be applied to the correlation orbitals. Of course, the key issue is that the correlation orbitals change the wavefunction in the region of maximum Laplacian, near the nucleus, so must be included in the computation. The virtue of one or the other of these approaches can only be justified by future appeal to experimental evidence, which will be in a subsequent publication. Here we note that in practice the improvement of the LCG-Welton is independent of this question and its answer. In a test computation on copper $K\alpha$, the choice of spectroscopic orbital sum versus a sum over all orbitals (spectroscopic and correlation) could lead to a shift of 0.4% of the self-energy contribution, and hence be secondary to the choice below.

During the RCI calculation process, the user is presented with multiple prompts for the inclusion of various relativistic corrections such as the transverse photon interaction and self-energy estimation.

It is generally recommended that all effects are included for more accurate results. In this update, Eq. (5) is now made the default option for self-energy calculation.

The original formulation for the evaluation of the self-energy of ground-state hydrogenic atoms was provided by Mohr (1974), which was later extended to include $n = 2$ hydrogenic systems (Mohr, 1983). Further developments in recent time have seen hydrogenic self-energies evaluated for $n = 3, 4, 5$ (Mohr and Kim, 1992; Indelicato et al., 1998; Le Bigot et al., 2001). Eq. (5) allows us to use these high accuracy hydrogenic computations to estimate the self-energy of a more complex system by scaling the results of the hydrogenic system. We use all these results to provide the latter term of Eq. (5). For $n > 5$ the new implementation sets the contribution to be zero, which is a good approximation for many purposes. Note that the first order term scales as $(Z\alpha)^4/n^3$.

The Fermi model for the nuclear charge distribution is useful for finite-difference methods because all derivatives are finite and continuous. The model is defined as

$$\rho(r) = \frac{\rho_0}{1 + e^{(r-c)/a}} \quad (9)$$

where a and c are constants relating to the nuclear size and skin thickness (the default values of a and c from the GENISO package of GRASP2K (Jönsson et al., 2007) were used for all following calculations).

By Poisson's equation, Parpia et al. (1996) defines the nuclear Laplacian as

$$\nabla^2 V(r) = \frac{\rho_0}{\epsilon_0 (1 + e^{(r-c)/a})} \quad (10)$$

which allows convenient numeric determination of $\nabla^2 V(r)$ for use in computation which we have implemented in this revision.

We also considered contributions to $V(r)$ from the mean electron distribution, since $\nabla^2 V(r)$ is proportional to the charge density. The nuclear Laplacian contributes a relative magnitude of Z over this nuclear region and the electronic screening (for 1s or 1s² occupations) contributes a relative magnitude of $(cZ/a_0)^3$ where the nuclear charge radius, c , is 2–4 Fermi, so the electronic contribution is negligible. As discussed in Grant (1980), the contribution from electronic charge distribution near the nucleus is some 4–6 orders of magnitude smaller than that from the nuclear charge distribution. We confirmed that computation of the electric charge Laplacian did not alter the self-energy screening, but did introduce a great deal of non-physical noise associated with the finite grid on which it was calculated. For this reason we have implemented the robust analytic approach based on nuclear Laplacian as given in Eq. (9).

The options are defined as follows:

1. No screening:

$$E_{SE,i}^1 = E_{SE,i}^H$$

2. Original GRASP2K screening:

$$E_{SE,i}^2 = \frac{\langle \psi_{i,r < 0.0219a_0} | \psi_{i,r < 0.0219a_0} \rangle}{\langle \psi_{i,r < 0.0219a_0}^H | \psi_{i,r < 0.0219a_0}^H \rangle} E_{SE,i}^H$$

3. Electron density screening at the origin:

$$E_{SE,i}^3 = \frac{\langle \psi_i(r \rightarrow 0) | \psi_i(r \rightarrow 0) \rangle}{\langle \psi_i^H(r \rightarrow 0) | \psi_i^H(r \rightarrow 0) \rangle} E_{SE,i}^H$$

4. Hydrogenic wavefunction projection:

$$E_{SE,i}^4 = |\langle \psi_i^H | \psi_i \rangle| E_{SE,i}^H$$

5. Lowe–Chantler–Grant–Welton method weighting:

$$E_{SE,i}^5 = \frac{\langle \psi_i | \nabla^2 V(\mathbf{x}) | \psi_i \rangle}{\langle \psi_i^H | \nabla^2 V(\mathbf{x}) | \psi_i^H \rangle} E_{SE,i}^H \quad (11)$$

Only our functional (Option 5) has a well-defined derivation from the Welton idea, with the others (Options 1–4) being generally poor estimates with poor mathematical basis. Option 2 and 3 also reflect a correction for the nuclear potential, and only options 2 and 5 include squared matrix elements and a nuclear size term. The screening coefficient used by the original GRASP2K package (Option 2) is the overlap integral of the wavefunction and a hydrogenic wavefunction in the region $r \leq 0.0219a_0$. Option 4 uses a monopole projection of the actual wavefunction onto a hydrogenic wavefunction. Option 3 is similar to the approach of Scofield (1973) in his calculation of the relativistic atomic form factor, which uses the ratio of the actual wavefunction density to that of a hydrogenic wavefunction at $r = 0$ as the screening coefficient. Although this approach is clearly incorrect, it represents a prior approach and has been used in older GRASP codes. The fifth option, now the default calculation, uses the theory introduced by Lowe et al. (2013) as has been discussed earlier. The wavefunctions (ψ) in these cases are for one-electron spinor, and therefore the energy, E , are for the matrix elements between the basis configuration state functions. ψ_i^H is the converged spinor for a one-electron system in orbital or quantum numbers, i . ψ_i is the same but for the many-electron system after convergence. It is perhaps obvious that this pair of computations requires two passes of normal GRASP coding. The shielded nuclear potential from the final converged wavefunctions is used in the calculation of self-energy.

3. Changes to the codes from v1.10

In order to facilitate the LCG-Welton self-energy screening method, some new subroutines were written while others were modified. For pre-existing subroutines and library files, they are copied with the suffix `_orig_v1_1` added. A separate folder for RCI 4 is created, leaving RCI 3 in its original form as presented in GRASP v1.1. This would provide users with more flexibility and greater choices.

4. Significance of self-energy: Results of isoelectronic sequence

4.1. Hydrogen-like isoelectronic sequence

The following is a comparison between our implementation and experimental results for hydrogen-like Ly- $\alpha_{1,2}$ transitions. The experimental results are scaled to be relative to theory. Horizontal offsets have been introduced for readability of the data points. It can be seen in Fig. 1 that there is generally excellent agreement between theory (and the new code) and experiment to within less than 0.5 eV.

4.2. Helium-like isoelectronic sequence

The helium-like system is one of the most extensively used systems in QED studies because it is the simplest possible three-body system. The effect of self-energy screening is most dominant in ground state terms that include the $1s^2$ configuration. Fig. 2 shows the results of screening contribution from a helium-like isoelectronic series redrawn from the original work of Lowe et al. (2013) relating to GRASP2K v1.0.

All four screening methods discussed in Section 2 have been compared with the results of other authors. These results were calculated using a single CSF configuration with no higher-order expansion. We note that the effect of additional higher-order expansions on the self-energy screening is expected to be minimal. The works of Yerokhin and Shabaev (1995) and Yerokhin et al. (1997) were based on partial-wave techniques, which was later extended by Artemyev et al. (2005). On the other hand, perturbation theory was used by Indelicato and Mohr (2001). Despite the different approaches used, all followed a similar trend. More importantly, the results using the LCG-Welton (Eq. (5)) method follows a similar pattern as opposed to the original GRASP2K screening method. In the range that is below approximate $Z = 30$,

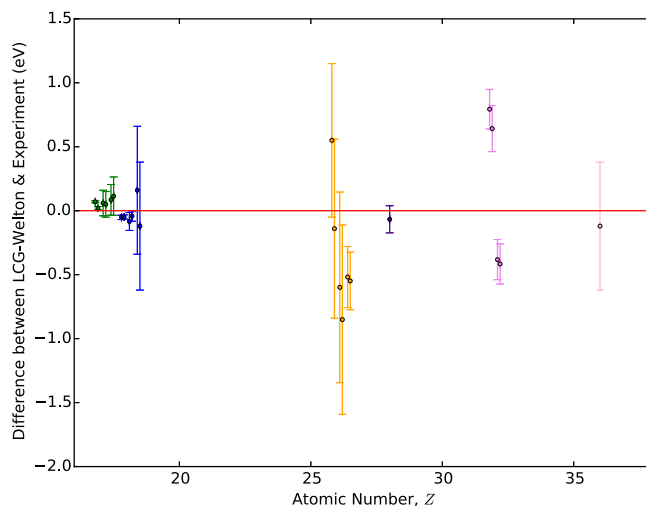


Fig. 1. Experimental results of H-like Lyman- $\alpha_{1,2}$ relative to theoretical calculations using LCG-Welton. Due to multiple data points sharing the same Z value, the results have been offset horizontally for readability. In order of Z , the references are: $Z = 17$: Richard et al. (1984), Källne et al. (1984), Deslattes et al. (1985); $Z = 18$: Beyer et al. (1985), Marmar et al. (1986), Briand et al. (1983); $Z = 26$: Briand et al. (1983), Silver et al. (1987), Chantler et al. (2007); $Z = 28$: Beyer et al. (1991); $Z = 32$: Laming et al. (1988), Chantler et al. (2009a).

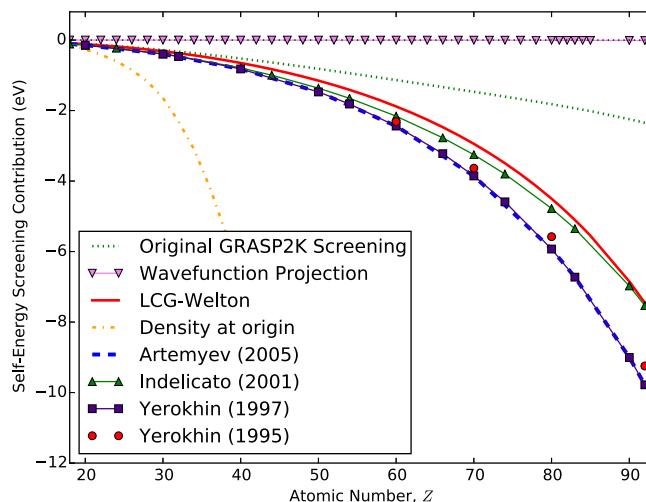


Fig. 2. Screening contributions to helium-like ground state self-energy $1s^2 \ ^1S_0$ (Lowe et al., 2013). The results between the alternative screening options are compared with those of other authors, which provide strong support for the method implemented here. The current state-of-the-art of theoretical comparison with good experimental support is given by Artemyev, and it is clearly seen that the current *ansatz* is much closer than earlier GRASP2K approaches.

the results using GRASP2K original screening method and LCG-Welton appear to agree quite well with each other and the literature. However, this is misleading as the energy axis is in eV, whereas to compare low atomic number we should, for example, scale as a fraction of the total self-energy. In particular, the fractional experimental accuracy for low atomic number can reach 10^{-14} for hydrogen and 10^{-6} for helium, so a useful implementation ought to approach that level. For hydrogenic systems our implementation achieves this by definition but for many electron systems including two-electron systems, the collection of advanced computations and predictions are as given in the plot.

When moving beyond $Z = 30$, the results from the GRASP2K original method diverges from the rest. For completeness, the results using the other non-default screening methods – namely nuclear density

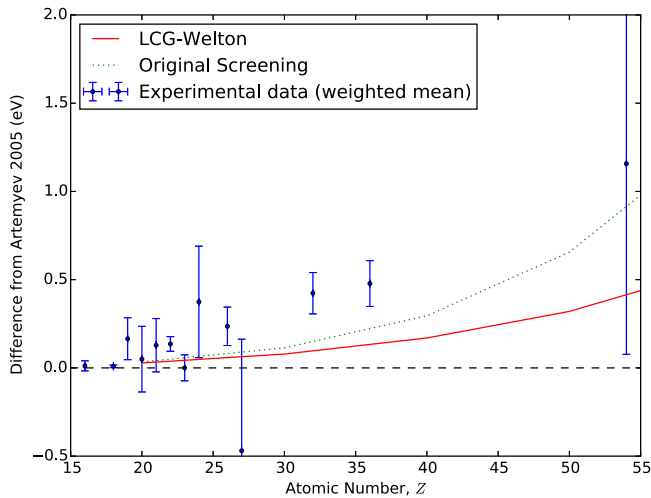


Fig. 3. Discrepancy of experimental data from the theory for two-electron systems of Artemyev (2005). The data plotted are weighted mean results for the w , x , y , and z transitions. The results of LCG-Welton are also plotted.

screening and hydrogenic wavefunction projection – are also included in Fig. 2. Further discussions of the non-default options are given below. The hydrogenic overlap approach – which predicts effectively zero screening – is a very poor prediction; and the nuclear overlap (electron density at the origin) overestimates the screening wildly. The new implementation follows the cluster of advanced theoretical results corresponding to Yerokhin et al. (1997), Artemyev et al. (2005) and Indelicato and Mohr (2001). Indelicato and Mohr (2001) provides a similar level of code and sophistication as we are discussing and indeed also uses the Welton idea in a similar but different qualitative and quantitative implementation.

Fig. 3 are weighted mean results of the $w(1s^2(^1S_0) - 1s2p(^1P_1))$, $x(1s^2(^1S_0) - 1s2p(^3P_2))$, $y(1s^2(^1S_0) - 1s2p(^3P_1))$, and $z(1s^2(^1S_0) - 1s2s(^3S_1))$ transitions relative to Artemyev (2005). The full list of reference for the experimental data are provided in Table 1. Included on the figure are also the results of the self-energy calculated using LCG-Welton, relative to Artemyev (2005).

For helium-like systems the resonance transitions to the ground state $1s^2$ have been measured to 10 parts per million (p.p.m.) or better across wide ranges of atomic number so that there is a good and reliable baseline for the comparison of the transition energies. For detailed summary and status on these transitions we refer to Chantler et al. (2012), Payne et al. (2014) and Chantler et al. (2014b). Amongst other conclusions, this implies that the comparison of experiment and theory is currently a very active area of interest. The current default prediction is that of Artemyev et al. as plotted in Fig. 2; and all experimental evidence is currently considered to lie somewhere between Artemyev et al. (2005) and a line not too far from that of Indelicato and Mohr (2001). The new implementation of LCG-Welton fits within the current experimental variability, with a maximum possible error of 0.1 eV around $Z = 40$, a maximum possible error of 0.2 eV at about $Z = 58$, and rising to a possible maximum error of about 2.5 eV at $Z = 92$. The experimental evidence permits us to claim an uncertainty (or error) of half these values, and there is some evidence that experimental data might lie closer to Eq. (4) and Option 5.

Irrespective of the detailed comparison with experiment, the current implementation and approximation is in good agreement with experiment across all atomic numbers, and that by comparison the earlier screening method is in disagreement with experiment across all atomic numbers. The magnitude of these effects can be considered in Table 2.

The total self-energy for a $1s$ electron can of course exceed 200 eV. While the original screening can have a magnitude up to 3 eV or 13

eV, the improved method can yield corrections of 11 eV or 20 eV for corresponding systems.

In hydrogen-like systems, the largest QED correction to the electron energy levels is the self-energy correction of order $(Z\alpha)^4$, and remains true for helium-like systems as well but with the addition of strong screening effects. Most experiments on QED are based on hydrogenic or helium-like systems, and recent advances have seen results with sub-eV accuracy, and indeed with 10 part per million accuracy. Therefore, the importance of improved approaches for self-energy and screening are high across all atomic numbers. Although these effects might appear minor for low- Z elements, percentage accuracy of experiment and theory is generally better at lower atomic number, and both Fig. 2 and Table 2 have illustrated that the effect cannot be ignored for mid- to high- Z .

B. Standard tests, benchmarks and options for advanced users

5. Evaluation of revised RCI program and packages

The dramatic advantages of the new method of calculation in relation to QED corrections have been demonstrated in detail by Lowe et al. (2013). In this manuscript we are particularly concerned with the coherent implementation and stability of the full package, so we choose examples which do not highlight the significance of the new approach but rather demonstrate its consistency and stability. We are interested in whether the new implementations adversely affect the results in any way. We have also performed the same tests on various other platforms to ensure that the results are independent of system architecture.

As part of our evaluation process, a select number of samples are calculated using the following set of codes:

- GRASP2K v1.0 with original RCI2 – Jönsson et al. (2007)
- GRASP2K v1.0 with RCI2 modified by Lowe et al. (2013)
- GRASP2K v1.1 with original RCI3 – Jönsson et al. (2013)
- GRASP2K v1.1 with RCI4 – This work, using the old implementation for comparison of consistency and stability.
- GRASP2K v1.1 with RCI4 – This work, using the new QED computation

In order to maintain parity and test stability in relation to the earlier versions of GRASP2K, we select for the main benchmark the original self-energy screening option, which of course is the only option available in (a) and (c). However for comparison purposes we also present the new implementation of the Welton idea. By performing the same calculation across the four sets of codes listed above, not only can we directly observe any effect that the revision would have had on the calculation, we can also see how the transition from v1.0 to v1.1 might have affected the results. The methods of testing and results for the different samples are outlined below in their respective sections. Here we provide a sample of prompts and inputs users can adopt for testing this benchmark. Full details of the procedures have been included as a shell script with the package which is located in /manual/benchmark/.

5.1. Sample inputs

In this study we have chosen not to use the default setting, which is now the LCG-Welton approach. This way, we can select other methods of screening. In this case, we have selected option 2 to replicate the original GRASP2K screening. During this process, relativistic corrections beyond the usual Dirac–Coulomb approximation for many-electron systems are implemented. The contribution from transverse photon interactions is included:

$$H_{\text{trans}} = - \sum_{i < j}^N \left[\frac{\alpha_i \cdot \alpha_j \cos(\omega_{ij} r_{ij})}{r_{ij}} + (\alpha_i \cdot \nabla_i)(\alpha_j \cdot \nabla_j) \frac{\cos(\omega_{ij} r_{ij}) - 1}{\omega_{ij}^2 r_{ij}} \right]. \quad (12)$$

Table 1
Experimental values used in analysis.

Measurement #	Z	Element	Line	Energy eV	σ eV	Discrepancy eV	Reference
1	16	S	w	2461.2735	0.4886	0.6443	Aglitskii et al. (1974)
2	16	S	w	2460.6874	0.1465	0.0582	Aglitsky et al. (1988)
3	16	S	w	2461.8000	3.0000	1.1708	Cocke et al. (1974)
4	16	S	w	2460.6410	0.0320	0.0118	Kubicek et al. (2009)
5	16	S	w	2460.6700	0.0900	0.0408	Schleinkofer et al. (1982)
6	16	S	y	2447.0500	0.1100	-0.0939	Schleinkofer et al. (1982)
7	18	Ar	w	3139.6000	0.2500	0.0179	Briand et al. (1983)
8	18	Ar	w	3139.5830	0.0630	0.0009	Bruhns et al. (2007)
9	18	Ar	w	3139.5517	0.0366	-0.0304	Deslattes et al. (1984)
10	18	Ar	w	3140.1000	0.7000	0.5179	Dohmann and Mann (1979)
11	18	Ar	w	3139.5810	0.0050	-0.0011	Kubicek et al. (2012)
12	18	Ar	w	3138.9000	0.9000	-0.6821	Neupert (1971)
13	18	Ar	x	3126.2830	0.0363	-0.0066	Deslattes et al. (1984)
14	18	Ar	y	3123.5208	0.0362	-0.0136	Deslattes et al. (1984)
15	18	Ar	z	3104.1480	0.0077	-0.0003	Amaro et al. (2012)
16	19	K	w	3511.4048	0.4972	0.9432	Aglitskii et al. (1974)
17	19	K	w	3510.5796	0.1229	0.1180	Beiersdorfer et al. (1989)
18	20	Ca	w	3902.4273	0.1860	0.0496	Aglitsky et al. (1988)
19	21	Sc	w	4315.5408	0.1510	0.1284	Beiersdorfer et al. (1989)
20	22	Ti	w	4750.1702	0.9100	0.5261	Aglitskii et al. (1974)
21	22	Ti	w	4749.7335	0.1662	0.0894	Beiersdorfer et al. (1989)
22	22	Ti	w	4749.8520	0.0720	0.2079	Chantler et al. (2012)
23	22	Ti	x	4733.8335	0.1311	0.0327	Payne et al. (2014)
24	22	Ti	y	4727.0667	0.1000	0.1294	Payne et al. (2014)
25	22	Ti	z	4702.0782	0.0723	0.1036	Payne et al. (2014)
26	23	V	w	5204.3904	1.0923	-0.7749	Aglitskii et al. (1974)
27	23	V	w	5205.5922	0.5464	0.4269	Aglitsky et al. (1988)
28	23	V	w	5205.2644	0.2082	0.0991	Beiersdorfer et al. (1989)
29	23	V	w	5205.1000	0.1400	-0.0653	Chantler et al. (2000)
30	23	V	x	5189.1200	0.2200	0.3822	Chantler et al. (2000)
31	23	V	y	5180.2200	0.1700	-0.1064	Chantler et al. (2000)
32	23	V	z	5153.8200	0.1400	-0.0762	Chantler et al. (2000)
33	24	Cr	w	5682.6562	0.5209	0.5878	Aglitsky et al. (1988)
34	24	Cr	w	5682.3176	0.3978	0.2492	Beiersdorfer et al. (1989)
35	26	Fe	w	6700.7617	0.3621	0.3270	Aglitsky et al. (1988)
36	26	Fe	w	6700.7254	0.2010	0.2907	Beiersdorfer et al. (1989)
37	26	Fe	w	6700.9000	0.2680	0.4653	Briand et al. (1984b)
38	26	Fe	w	6700.4025	0.3172	-0.0322	Chantler et al. (2007)
39	26	Fe	x	6682.7000	0.2673	0.3661	Briand et al. (1984b)
40	26	Fe	y	6667.5000	0.2667	-0.0786	Briand et al. (1984b)
41	27	Co	w	7241.6439	0.6323	-0.4694	Aglitsky et al. (1988)
42	32	Ge	w	10280.3573	0.2715	0.1398	Chantler et al. (2009b)
43	32	Ge	w	10280.7000	0.2200	0.4825	MacLaren et al. (1992)
44	32	Ge	x	10259.5155	0.3693	0.6416	MacLaren et al. (1992)
45	32	Ge	y	10220.9316	0.2275	0.1320	Chantler et al. (2009b)
46	32	Ge	y	10221.7911	0.3475	0.9915	MacLaren et al. (1992)
47	32	Ge	z	10181.3324	0.5192	0.9456	MacLaren et al. (1992)
48	36	Kr	w	13113.8000	1.2000	-0.6705	Briand et al. (1984a)
49	36	Kr	w	13115.4500	0.3000	0.9795	Indelicato et al. (1986)
50	36	Kr	w	13114.7800	0.7100	0.3095	Widmann et al. (1995)
51	36	Kr	w	13114.6800	0.3600	0.2095	Widmann et al. (1996)
52	36	Kr	x	13091.5300	0.8200	0.6643	Widmann et al. (1995)
53	36	Kr	x	13091.1700	0.3700	0.3043	Widmann et al. (1996)
54	36	Kr	y	13026.8000	0.3000	0.6835	Indelicato et al. (1986)
55	36	Kr	y	13026.3000	0.7100	0.1835	Widmann et al. (1995)
56	36	Kr	y	13026.2900	0.3600	0.1735	Widmann et al. (1996)
57	36	Kr	z	12979.7200	0.6600	0.4544	Widmann et al. (1995)
58	36	Kr	z	12979.6300	0.4100	0.3644	Widmann et al. (1996)
59	54	Xe	w	30629.1000	3.5000	-0.9512	Briand et al. (1989)
60	54	Xe	w	30631.2000	1.2000	1.1488	Thorn et al. (2009)
61	54	Xe	y	30209.6000	3.5000	3.3348	Briand et al. (1989)

The frequency of the transverse photon, ω_{ij} , used here is taken to be the difference in the diagonal Lagrange multipliers associated with the orbitals. In general, this is an appropriate approximation for spectroscopic

and singly occupied orbitals, but is not necessarily true when correlation orbitals are present. Therefore, the transverse photon interaction is computed in the low-frequency limit ($\omega_{ij} \rightarrow 0$), often referred to as

Table 2

Total self-energy contribution to a $1s$ orbital (column 2) and total self-energy screening contribution to helium-like copper, xenon, and uranium. The difference of the screening between the two methods (LCG-Welton and original GRASP) become much larger as Z increases, which is demonstrated in Fig. 2. Current experimental evidence is in agreement with LCG-Welton within uncertainty and in disagreement with the original GRASP screening.

	$1s$ Self-Energy in Helium-like Systems and Self-Energy Screening (eV)		
	$1s$ (unscreened)	Screening LCG-Welton	Original GRASP
Copper	6.2030	0.2926	-0.2624
Xenon	51.0331	1.4120	-0.9413
Uranium	359.4764	7.4540	-2.3470

the Breit interaction. The Breit interaction is computed perturbatively instead of incorporated self-consistently within the Hamiltonian. Since is a first-order effect, the difference between a perturbative approach and self-consistent method is minimal (Chantler et al., 2014a).

The normal mass shift in the lowest-order correction for nuclear motion is

$$H_{\text{NMS}} = \frac{1}{m_{\text{nuc}}} \sum_i T_i, \quad (13)$$

with T_i the usual Dirac kinetic energy operator, whilst the specific mass shift is taken to be the coupling of the electron and nuclear motions,

$$H_{\text{SMS}} = \frac{1}{m_{\text{nuc}}} \sum_{i < j} \mathbf{p}_i \cdot \mathbf{p}_j. \quad (14)$$

A more elaborate treatment of the relativistic isotope shift is available via an additional module, RIS3 (Nazé et al., 2013), which is compatible with GRASP2K v1.1. From the test run for He-like copper, xenon, and uranium, the hydrogenic wavefunction is generated by the script `sh_hydrogenic`, which generates the relevant files which in this case we named `hydrogenic_wavfn`. This is ψ_i^H . The He-like samples are generated as single configuration states and named appropriately, for example, `he_1s_uranium`. An example of a RCI3 run using LCG-Welton on Ne II is provided in Appendix B. Note that using LCG-Welton self-energy screening is now the default option. This example is extracted from the neon test calculation. A script for this can be found in the directory `/manual/benchmark/`.

If the user wishes to use any other screening method, including the original GRASP screening method, then they have to choose non-default method for self-energy screening. An illustration of this can be found in Appendix C.

5.2. Neon II

This is a simple calculation in which we monitored the eigenenergies of Ne II ($1s^1 2s^2 2p^6$) during a multiconfiguration calculation. We constructed Ne II by building up the orbitals systematically, beginning with the $1s^1$ core, then expanded to $2s^2 2p^6$ and subsequent multiconfiguration calculations. The eigenenergies were monitored after the atom has been constructed. No transition calculation was performed for this set. Our calculations and methodology are detailed in the sample script given for neon that comes with the package. Although written for RCI4, the technique is very much the same for the others. More explicitly: We first calculated $1s$, then $2s 2p$. In both steps, we have allowed all orbitals to be active. Expand to $3s 3p 3d$. Allow all orbitals to be active except for $1s$, which is kept inactive. Similarly, expand to $4s 4p 4d 4f$, allowing all orbitals to be active except for $1s$, which is kept inactive. The results for Ne II (Table 3) are relatively stable with little variations amongst the different versions used. In fact, there is negligible difference between the (a) original GRASP2K v1.0, and (b) Lowe's modification of GRASP2K v1.0. The same can be said for GRASP2K v1.1 with RCI3 and this work (v1.1 with RCI4). The main difference is between GRASP2K v1.0 and v1.1. We expect that the corrections of version 1.1 are important and are a cause for the eigenvalue shifts, but we do not here push this computation to convergence nor compare to advanced experimental work to define

a more accurate approach — this would be a complex issue beyond the mandate of benchmark testing. It is sufficient to note the scale and magnitude of the typical shifts. The self-energy corrections for oxygen, $Z = 8$ and neon $Z = 10$ are quite small, about 0.001–0.003 eV respectively, and more significant figures are needed to reveal the differences between implementations, with main variation in the tables dominated by numerical convergence and improvements of the angular momentum code.

5.3. Oxygen

For this part of the test, we seek to investigate the effect of the revision on forbidden transitions. This set of calculation involves the famous forbidden green line (557 nm) observed in the aurora, believed to be the result of the transition $1s^2 2s^2 2p^4 \ ^1S_0 - 1s^2 2s^2 2p^4 \ ^1D_2$. The method of calculation used for this set is identical to the technique presented by Chantler et al. (2013). That is, the orbitals are built up by the principal quantum number, n , with the core inactive whilst allowing a maximum of 2 electrons to be excited. Results for the A-coefficient are reported in both length (Babushkin) and velocity (Coulomb) gauges (Table 4).

Similar to the results of Neon II, these results of oxygen show no major variation between the two versions of GRASP2K v1.0, namely (a) and (c). Comparing (c) and this work, the results are virtually identical with an extremely small difference in the A-coefficients. This difference, although extremely small, is most prominent when using the velocity gauge. The velocity gauge is generally less stable than its counterpart in the length gauge, especially at the preliminary stage of multiconfiguration calculations. The stability of the results in the length gauge across the different versions appears to support this idea. Forbidden transitions such as this are notoriously sensitive and prone to issues of stability and convergence. However, the purpose of the current investigation is to test the stability of the new QED implementations. Therefore, the obvious difference between the length and velocity gauge is not a concern here, as further expansion towards a larger set of configuration state function should, ideally, resolve such convergence issues. This topic has been discussed in detail by Chantler et al. (2013).

5.4. Copper

The transition we have chosen for this test is $\text{Cu-}K\alpha$. This is an allowed electric dipole transition of a heavier element. In this set of calculations, we have adopted the technique of Chantler et al. (2010) (referred to as Method 1) where the reference configuration is divided into a set of inactive core orbitals ($1s$, $2s$, $2p$) and an active set of valence orbitals ($3s$, $3p$, $3d$, $4s$). Similar to the case of oxygen, we allowed a maximum of 2 excitations.

The results of $\text{Cu-}K\alpha$ (Table 5) present an interesting insight into the effect of the modifications made to the former revision for v1 and its incarnation, which is the revision for v1.1 presented in this work. Since this is a relatively strong electric dipole transition, there is no significant issue with the convergence of the two gauges like ones we have seen with the electric quadrupole transition in oxygen. This is clearly demonstrated by the ratio of length to velocity gauge (L/V). Unlike with forbidden transitions, the excellent convergence of the two

Table 3

Consistency and null test: Eigenenergies for Neon II calculations using the four different versions of GRASP2K on platform 1. Results between the two versions 1.0 suggests that the implementation of the new theory does not affect the results of the older version. This is also the case between version 1.1 using RCI3 and RCI4 (original screening). There is a small difference between the original GRASP screening and LCG-Welton approach when relativistic effects are added at the RCI level. (a) Jönsson et al. (2007) (b) Lowe et al. (2013) (c) Jönsson et al. (2013). As this is a low-Z element, the small difference between the original screening and LCG-Welton approach is of order 0.0002 eV.

Neon Expansion	GRASP2K 1.0 (a)	GRASP2K 1.0 (b)	v1.1 (RCI3) (c)	v1.1 (RCI4) Original screening	v1.1 (RCI4) LCG-Welton
2p (no RCI, no QED)	-2 631.0942 eV	-2 631.0942 eV	-2 632.0931 eV	-2 632.0931 eV	-2 632.0931 eV
3d (RCI)	-2 638.0840 eV	-2 638.0840 eV	-2 638.0829 eV	-2 638.0829 eV	-2 638.0831 eV
4f (RCI)	-2 639.7348 eV	-2 639.7348 eV	-2 639.7337 eV	-2 639.7337 eV	-2 639.7339 eV

Table 4

Consistency and null test: Results of the preliminary calculation of the oxygen transition thought to be responsible for the 557 nm green line seen in the aurora. (a) Jönsson et al. (2007) (b) Lowe et al. (2013) (c) Jönsson et al. (2013). We do not expect significant changes to the transition energies or A-coefficients in these tests and indeed the results are stable. The self-energy corrections for oxygen, $Z = 8$ and neon $Z = 10$ are quite small, about 0.001–0.003 eV respectively, and more significant figures are needed to reveal the differences between implementations, with main variation in the tables dominated by numerical convergence and improvements of the angular momentum code of GRASP2K 1.1 (RCI3) and this work using RCI4. For completeness, the A-coefficient is reported in both length (Babushkin) and velocity (Coulomb) gauges. It is well established that obtaining gauge convergence with forbidden transitions such as this can be more difficult than regular electric dipole transitions. In many cases, convergence is much slower and requires a larger basis set than comparable electric dipole transitions. As the purpose of here is to test the stability of the QED implementation, obtaining convergence of the gauges is not within the scope of the current work. The 557 nm green line forbidden transition and the consequences of gauge convergence has previously been investigated by Chantler et al. (2013).

Oxygen	GRASP2K				
	1.0	1.0	1.1 (RCI3)	1.1 (RCI4)	1.1 (RCI4)
3d Expansion	(a)	(b)	(c)	Original screening	LCG-Welton
Energy (eV)	2.174	2.174	2.174	2.174	2.174
	Transition rate (A-coefficient), s^{-1} :				
Length Gauge (B)	1.13276	1.13276	1.13276	1.13277	1.13277
Velocity Gauge (C)	4.87572 E-03	4.87572 E-03	4.87578 E-03	4.87566 E-03	4.87558 E-03
L/V Ratio	232.327	232.327	232.324	232.332	232.335
4f Expansion					
Energy (eV)	2.229	2.229	2.229	2.229	2.229
	Transition rate (A-coefficient), s^{-1} :				
Length Gauge (B)	1.25140	1.25140	1.25140	1.25141	1.25140
Velocity Gauge (C)	6.15446 E-01	6.15446 E-01	6.15444 E-01	6.15450 E-01	6.15448 E-01
L/V Ratio	2.03	2.03	2.03	2.03	2.03

Table 5

Results for Cu- $K\alpha$. The difference from the original GRASP2K (a) is possibly due to developments from the original code, addressed in (c). Keys: (a) Jönsson et al. (2007) (b) Lowe et al. (2013) (c) Jönsson et al. (2013). Cu- $K\alpha$ is one of the most widely used spectra in X-ray investigations, making it an appropriate choice for benchmark testings. Significant differences in the transition energies can be seen between (a) and (b) but these appear more in the nature of convergence issues than variation of self-energy (Lowe et al., 2013). Using the original GRASP screening method as implemented in RCI4, we can see that there is hardly any change to the results of version 1.1 (RCI3). Hence it appears that version 1.1 overall is more stable than the earlier 1.0. The LCG-Welton screening yields a small increase in transition energy of roughly 0.03 eV. We emphasise that these results are not final high-accuracy calculations, but are from simple test procedures with the purpose of providing benchmarks for comparison between the various versions on the grounds of stability and consistency.

Cu- $K\alpha$	GRASP2K				
	1.0	1.0	1.1 (RCI3)	1.1 (RCI4)	1.1 (RCI4)
4s Expansion	(a)	(b)	(c)	Original screening	LCG-Welton
Energy (eV)	8050.78	8050.91	8047.13	8047.13	8047.17
	Transition rate (A-coefficient), s^{-1} :				
Length Gauge (B)	6.10994 E+14	6.11144 E+14	6.10293 E+14	6.10294 E+14	6.10301 E+14
Velocity Gauge (C)	6.06535 E+14	6.06623 E+14	6.06349 E+14	6.06349 E+14	6.06351 E+14
L/V Ratio	1.00735	1.00745	1.00650	1.00650	1.00651
4f Expansion					
Energy (eV)	8047.40	8046.70	8048.19	8048.20	8048.23
	Transition rate (A-coefficient), s^{-1} :				
Length Gauge (B)	6.03826 E+14	6.03777 E+14	6.07313 E+14	6.07314 E+14	6.07321 E+14
Velocity Gauge (C)	5.99879 E+14	5.99933 E+14	6.03223 E+14	6.03224 E+14	6.03226 E+14
L/V Ratio	1.00658	1.00641	1.00678	1.00680	1.00679
5s Expansion					
Energy (eV)	8046.92	8046.53	8048.33	8048.33	8048.36
	Transition rate (A-coefficient), s^{-1} :				
Length Gauge (B)	6.03751 E+14	6.03594 E+14	6.07077 E+14	6.07077 E+14	6.07085 E+14
Velocity Gauge (C)	5.99721 E+14	5.99777 E+14	6.02969 E+14	6.02969 E+14	6.02971 E+14
L/V Ratio	1.00672	1.00636	1.00681	1.00681	1.00682

Table 6

Self-energy of the diagram transition of copper K α . Calculations are based on our current code. Given convergence issues, this is consistent with the evaluation earlier.

	Self-energy of Copper K α diagram transition (eV)		
	Total Self-energy, eV Upper State	Lower State	Transition
Copper	13.593	7.799	5.793
	Total Transition Energy without Self-Energy	with self-energy (Table 5)	Difference
Copper	8052.912	8047.17	5.74

gauges for the Cu-K α can be observed from as early as the 4s expansion. With this result, along with those for oxygen, we are confident that the new revision is robust and stable.

The differences between (a) and (b), even though they may appear to be minor, are in fact quite significant, especially for users interested in high-accuracy calculations. This is especially true when the energy differences can be up to 0.70 eV apart (4f expansion) or 0.39 eV (5s expansion). Some issues observed in (a) have been rectified in the recent update (c) and also in the patch by (b). The difference between v1.0 and 1.1 is, and should be, welcome because significant changes have been made to resolve and enhance various issues which required revision of v1.0 and which are outlined in detail in Jönsson et al. (2013).

The results, as outlined in Table 5, show that there is virtually no difference between the v1.1 (RCI3) and v1.1 (RCI4) using the original screening method. The excellent agreement between the two versions, (c) and this work, reinforces our earlier hypothesis that the difference between (a) and (b) was due to the instability of v1.0. Although such significant differences are not seen in the Neon II and oxygen calculation, this is likely due to the nature of this revision and the problem chosen. This revision provides an additional technique for calculating QED, which can be seen more easily amongst the heavier elements as opposed to the lighter ones. Since oxygen and neon are lower atomic number elements, effects from QED require higher accuracy when compared with copper. As a separate confirmation, we note from Table 6 that the self-energy contribution to any transition can be evaluated from those of the upper and lower states, given the level of detail of the GRASP2K computation and CSFs, and indeed is at least as accurate as the eigenvalue convergence observed. Recent extensive theoretical calculations by Nguyen et al. (2022b,a) on copper K α and K β diagram lines as well as satellite transitions with stability and accuracy up to 0.03 eV and near-unity gauge convergence provides further evidence of the robustness of the current code with the LCG-Welton implementations.

At this time we would recommend use of GRASP2K v1.1 (RCI4), with the default LCG-Welton screening, for all computations, though further critical investigation of this will doubtless be required with comparison to advanced experimental work. Further details of the importance of LCG-Welton screening are provided in Lowe et al. (2013). In particular, major differences are found in Figures 4–9 of that work, where the earlier screening method fails above atomic numbers around $Z = 30, 70, 40, 25$ depending upon the state or transition investigated.

5.5. Further test on alternative platforms

We have also performed the same tests as above on a few other platforms to ensure that this update is compatible with a variety of system architecture (Tables 6–10).

Platform 1: Ubuntu 12.04.5 LTS, Intel Core i7-4770 3.40 GHz, 8 GB RAM.

Platform 2: 14.04.2 LTS, Intel Core i7-2600K 3.40 GHz, 8 GB RAM.

Platform 3: Ubuntu 12.04 LTS, Intel Core i7-3610QM 2.30 GHz x 8, 8 GB RAM

The results calculated using versions 1.1 and this work on platform 2 are identical to those calculated above with platform 1. We did notice

some minor differences with results calculated on platform 3 using versions 1.0 (without the QED implementation) and 1.1. However, these variations are sufficiently small, and hence we have attributed them to the minor difference in the architecture of the compiler and system in question. Conversely, we have obtained exactly identical results for v1.1 (RCI4) across all three platforms.

6. Gauge parameter and the bioscl program

The generalised relativistic matrix element describing an electric multipole transition from state α to β currently used by the GRASP2K source code is

$$\mathbf{M}_{\alpha\beta}^e(\omega; G_L) = \mathbf{M}_{\alpha\beta}^e(\omega; 0) + G_L \mathbf{M}_{\alpha\beta}^l(\omega) \quad (15)$$

where ω is the photon frequency, and G_L is the gauge parameter. The superscripts e and l indicate the electric and magnetic components of the matrix element. A full explanation of the above equation and the associated theory has been provided by Grant (1974).

The constant G_L takes on the value of $G_L = 0$ for the velocity (Coulomb) gauge, and $G_L = \sqrt{(L+1)/L}$ for the length (Babushkin) gauge. The L represents the multipole order. At present, this is the method in which GRASP2K uses to calculate the transition rates in the two gauges. The gauge dependence of transition rates has been explored earlier by Gaigalas et al. (2010, 2012). In this revision, we explore a similar idea by adding a variable δ to Eq. (15), such that it now becomes

$$\mathbf{M}_{\alpha\beta}^e(\omega; G_L) = \mathbf{M}_{\alpha\beta}^e(\omega; 0) + \delta G_L \mathbf{M}_{\alpha\beta}^l(\omega) \quad (16)$$

which can be varied by users wishing to explore further into this topic. A prompt would appear at the relevant section when running the bioscl3 program asking the user whether they would like to use the default gauge scaling factor. If the input is yes, then $\delta = 1$ and nothing further is required. However, should the user selects no, then an additional prompt would require the user to enter a value for δ . In this latter case (non-default δ), the output would still have the label B to indicate that it is Babushkin, but it is not a true Babushkin gauge. Rather, it is now merely a ‘pseudo-Babushkin’ gauge. This addition should give the user more flexibility and the opportunity to investigate convergence.

7. Discussion

Although not previously offered publically nor published, but introduced as a patch for GRASP2K_v1.0 (Lowe et al., 2013), the LCG-Welton model has been shown to be a valid approach for QED self-energy and an important development and approximation. As such, it has seen wide usage across the literature, and in some instances, implemented in several other atomic structure codes such as DBSR_HF (Zatsarinny and Froese Fischer, 2016). We have demonstrated that our new implementation improves upon the original GRASP2K self-energy screening contribution, which brought it in line with other contemporary theories (Fig. 2). Our implementation compares well with experimental results for hydrogenic and helium-like systems, for example, with much less than 0.5 eV discrepancy for hydrogenic Ly- $\alpha_{1,2}$

transitions (Fig. 1) to $Z = 40$, even at $Z = 92$ for helium-like systems (Fig. 2). These particular systems follow most QED experiments, based on hydrogenic and helium-like systems, with extremely high accuracies (Chantler et al., 2012; Payne et al., 2014; Chantler et al., 2014b).

Extensive studies have been conducted to higher- Z by other authors with interesting results. Rzakiewicz et al. (2018) found that the theoretical results using the MCDHF method with the LCG-Welton self-energy correction is consistent with their high-accuracy EBIT experimental results on nickel- (W^{46+}) and copper-like (W^{45+}) tungsten ions to within less than 2.5 mÅ. The authors noted that the accuracy and consistency achieved theoretically using this method also relies heavily on the convergence of a high level of active set expansion – in this case, up to $n = 7$ – which may not always be achievable for complex, open-shell atoms.

Li et al. (2018) investigated the viability of using the transition $2p^5 2P_{3/2} -^2 P_{1/2}$ for ions in the F-like isoelectronic sequence as a testing ground for QED and the Breit effect. As such, a high-accuracy theory is desirable. The authors tested a number of different computational packages for atomic structure, which include GRASP2K_v1.1 of Jönsson et al. (2013), the LCG-Welton patch of Lowe et al. (2013) applied to GRASP2K_v1.0 (Jönsson et al., 2007), and the Model QED package of Shabaev et al. (2015). The LCG-Welton approach remain consistent with experiment overall. Conversely, the Model QED method of Shabaev et al. (2013) displayed larger discrepancies than expected. The authors pointed out various issues associated with the experimental data and suggested further studies be made experimentally and theoretically. The particular transition that Li et al. (2018) were investigating is a magnetic dipole ($M1$) transition, which is often difficult to calculate or measure accurately (Chantler et al., 2013).

Si et al. (2018) investigated Co-like ions and the transition $3d^9 2D_{3/2} -^2 D_{5/2}$. They used the same three testing platforms as Li et al. (2018) and reached a similar conclusion that there is consistency between the original GRASP2K and the modified LCG-Welton patch of Lowe et al. (2013). The difference between the three implementations are generally of the order of around 0.0025% to 0.015%. In all situations, however, the theoretical results fall outside the extremely small error bars of experimental results. The authors concluded that the Model QED package of Shabaev et al. (2015) can produce results that are closer to experimental data than results calculated using GRASP + LCG-Welton. The work of Si et al. (2018) on Co-like ions begin from $Z = 28$. The large deviation at low- Z from using the Model QED as reported by Li et al. (2018) was later investigated by Volotka et al. (2019), where it was concluded that the discrepancies could potentially be resolved if the calculations had included *ab initio* QED corrections. However, Shabaev et al. (2020) argued that it is the methodology of implementing the model Lamb shift operator (Shabaev et al., 2013) that can lead to discrepancies. However, Volotka et al. (2019) focused on F-like ions with $Z \geq 18$ whereas Shabaev et al. (2020) revisited the problem for F-like molybdenum and uranium. The problems seen with low- Z that was pointed out by Li et al. (2018) remains unresolved.

The conclusions of Li et al. (2018) are reinforced by Lu et al. (2020) and Zhang et al. (2020). Lu et al. (2020) measured the fine splitting structure of $2p^5$ in S^{7+} and Cl^{8+} , which are F-like ions. Their focus was on $10 \leq Z \leq 18$. Zhang et al. (2020) investigated silicon-like tungsten (W^{58+}) and like Rzakiewicz et al. (2018), also concluded that the calculations using the original GRASP2K tend to underestimate experiment, which was also observed previously by other authors. The application of LCG-Welton appears to have shifted the results closer to experimental values. Curiously, the results calculated using the Model QED approach tend to overestimate, which means that experimental results often fall between the two methods.

Clearly more work is required experimentally and theoretically; and also it is important to recognise the separate corrections for QED self-energy, vacuum-polarisation and the approach to Breit terms. Hence we encourage all to make use of the LCG-Welton approach where appropriate, to recognise appropriate limitations, and to note that there are many implementations of ‘Welton’s idea’, hence it is useful to label the relevant approach and implementation, in this case LCG-Welton.

8. Conclusion

A revised GRASP2K has been presented with improved techniques for the calculation of self-energy. The work is built upon GRASP2K v1.1, with appropriate benchmark test and results included. The results show consistency and overall improvement, especially in the high- Z regime where QED effects are significant. Extensive testing has shown that the LCG-Welton improves upon the original GRASP2K self-energy screening and compares favourably with experimental results. Alternative screening methods are also available for the more advanced users, as well as an option to further investigate the gauge dependence of transition rates. All citations to this work should also refer to the original work of GRASP2K v1.1 by Jönsson et al. (2013), and to this manuscript.

Declaration of competing interest

The authors declare the following financial interests/personal relationships which may be considered as potential competing interests: Co-author (C T Chantler) currently serves as an editor-in-chief for Radiation Physics and Chemistry.

Data availability

The code is available for download as part of the paper, in the supplementary zip with installation instructions.

Acknowledgements

We would like to acknowledge the community of GRASP users who have encouraged and cited this research, and especially P. Jönsson, G. Gaigalas, J. Bieroń, and C. Froese-Fischer for helpful advice in the preparation of this work. The authors would like to acknowledge the Australian research Council grant DP210100795.

Appendix A. Installation

The installation process of this revised version require the user to first set the appropriate environment, as detailed in the installation instructions of GRASP2K v1.1 (Jönsson et al., 2013). The .tar.gz should be extracted to the same folder as GRASP2k v1.1. The installation process can be initiated by executing the script `install_package`. Further details can be found in the associated README file. All tests and results reported in this paper were performed on Linux systems using the `gfortran` compiler. Citations to this work should also refer to the original work of GRASP2K v1.1 by Jönsson et al. (2013).

Appendix B. Example of running RCI using LCG-Welton self-energy screening

```
=====
RCI4: Execution Begins ...
=====
Default settings? y
Name of state: Neon3d
isofile = isodata
name = Neon3d
Block      1 , ncf =      149
Loading CSL file ... Header only
There are/is      9 relativistic subshells;
Calling SETRES...
Include contribution of H (Transverse)?
y
Modify all transverse photon frequencies?
n
```

```

Include H (Vacuum Polarisation)?
y
Include H (Normal Mass Shift)?
y
Include H (Specific Mass Shift)?
y
Estimate self-energy?
y
Default method for self-energy calculation?
y
Name of hydrogenic wavefunctions state: hydrogenic_wavefn
name = hydrogenic_wavefn
Loading Radial WaveFunction File ...
Calling SETMIX...
There are      1 blocks (block J/Parity NCF):
1 1/2+ 149

Enter ASF serial numbers for each block
Block      1 ncf =      149 id = 1/2+
1

```

Appendix C. Example of running RCI using other self-energy screening methods

```

=====
RCI4: Execution Begins ...
=====
Default settings? y
Name of state: Neon3d
isofile = isodata
name = Neon3d
Block      1 , ncf =      149
Loading CSL file ... Header only
There are/is      9 relativistic subshells;
Calling SETRES...
Include contribution of H (Transverse)?
y
Modify all transverse photon frequencies?
n
Include H (Vacuum Polarisation)?
y
Include H (Normal Mass Shift)?
y
Include H (Specific Mass Shift)?
y
Estimate self-energy?
y
Default method for self-energy calculation?
n
Enter name of state: Neon3d
Choose screening method:
1 -- No Screening
2 -- Original GRASP2K screening
3 -- Nuclear density screening
4 -- Hydrogenic wavefunction projection
5 -- LCG-Welton method weighting
2
Write screening debug output?
n

```

Appendix D. Supplementary data

The package is delivered in a `tar.gz` file and is designed to be unpacked and operational on a Linux system. The main folder contains the following folders and files:

1. `bin`
2. `examples`
3. `lib`
4. `manual`
5. `src`
6. `README` – which contains instructions on how to install the software
7. 3 `make-environment` files used to define the path, per the instructions in the `README` file

Furthermore, the package contains new examples designed to demonstrate the stability and consistency of the newly-implemented LCG-Welton self-energy screening method in GRASP2K_v1.1, as well as illustrating how to apply such method in the atomic structure calculations. The tests available are for copper, neon, and oxygen. Moreover, there is also a folder for helium-like systems, which includes He-like copper, uranium, and xenon. The script files to automate these calculations are included in the folder `benchmark`, located within the folder `manual`.

List of folders and files included in the `benchmark` folder:

1. `copper_v3` (53 files)
2. `neon_v3` (18 files)
3. `oxygen_v3` (21 files)
4. `he_like` (3 folders)
 - (a) `copper` (4 files)
 - (b) `uranium` (4 files)
 - (c) `xenon` (4 files)

Supplementary material related to this article can be found online at <https://doi.org/10.1016/j.radphyschem.2022.110644>.

References

- Aglietskii, E.V., Boiko, V.A., Zakharov, S.M., Pikuz, S.A., Faenov, A.Y., 1974. Observation in laser plasmas and identification of dielectron satellites of spectral lines of hydrogen- and helium-like ions of elements in the Na–V range. *Sov. J. Quantum Electron.* 4 (4), 500–513.
- Aglietskii, E.V., Antsiferov, P.S., Mandelstam, S.L., Panin, A.M., Safronova, U.I., Ulitin, S.A., Vainshtein, L.A., 1988. Comparison of calculated and measured wavelengths of resonance transitions in He-like ions for $Z=16-39$. *Phys. Scr.* 38, 136–142.
- Amaro, P., Schlessler, S., Guerra, M., Le Bigot, E.-O., Isac, J.-M., Travers, P., Santos, J.P., Szabo, C.I., Gumberidze, A., Indelicato, P., 2012. Absolute Measurement of the Relativistic Magnetic Dipole Transition Energy in Heliumlike Argon. *Phys. Rev. Lett.* 109, 043005–1–5.
- Artemyev, A.N., Shabaev, V.M., Yerokhin, V.A., Plunien, G., Soff, G., 2005. QED calculation of the $n = 1$ and $n = 2$ energy levels in He-like ions. *Phys. Rev. A* 71, 062104. <http://dx.doi.org/10.1103/PhysRevA.71.062104>.
- Beiersdorfer, P., Bitter, M., von Goeler, S., Hill, K.W., 1989. Experimental study of the x-ray transitions in the heliumlike isoelectronic sequence. *Phys. Rev. A* 40, 150–157.
- Beyer, H.F., Deslattes, R.D., Folkmann, F., La Villa, R.E., 1985. Determination of the 1s lamb shift in one-electron argon recoil ions. *J. Phys. B* 18, 207.
- Beyer, H.F., Indelicato, P., Finlayson, K.D., Liesen, D., Deslattes, R.D., 1991. Measurement of the 1s lamb shift in hydrogenlike nickel. *Phys. Rev. A* 43, 223–227.
- Briand, J.P., Indelicato, P., Simionovici, A., Vicente, V.S., Liesen, D., Dietrich, D., 1989. Spectroscopic study of hydrogenlike and heliumlike Xenon ions. *Europhys. Lett.* 9 (3), 225–230.
- Briand, J.-P., Indelicato, P., Tavernier, M., Gorceix, O., Leisen, D., Beyer, H.F., Liu, B., Warczak, A., Desclaux, J.P., 1984a. Observation of hydrogenlike and heliumlike krypton spectra. *Z. Phys. A* 318, 1.
- Briand, J.P., Mossé, J.P., Indelicato, P., Chevallier, P., Girard-Vernhet, D., Chetoui, A., Ramos, M.T., Desclaux, J.P., 1983. Spectroscopy of hydrogenlike and heliumlike argon. *Phys. Rev. A* 28, 1413–1417. <http://dx.doi.org/10.1103/PhysRevA281413>.

- Briand, J.P., Tavernier, M., Marrus, R., Desclaux, J.P., 1984b. High-precision spectroscopic study of heliumlike iron. *Phys. Rev. A* 29, 3143–3149. <http://dx.doi.org/10.1103/PhysRevA293143>.
- Bruhns, H., Braun, J., Kubicek, K., Lopez-Urrutia, J.R.C., Ullrich, J., 2007. Testing QED screening and two-loop contributions with He-like ions. *Phys. Rev. Lett.* 99, 113001–1–4. <http://dx.doi.org/10.1103/PhysRevLett99113001>.
- Chantler, C.T., Kinnane, M.N., Gillaspay, J.D., Hudson, L.T., Payne, A.T., Smale, L.F., Henins, A., Pomeroy, J.M., Tan, J.N., Kimpton, J.A., Takacs, E., Makonyi, K., 2012. Testing three-body quantum electrodynamics with trapped Ti^{20+} ions: Evidence for a Z-dependent divergence between experiment and calculation. *Phys. Rev. Lett.* 109, 153001–1–5.
- Chantler, C.T., Laming, J.M., Dietrich, D.D., Hallett, W.A., McDonald, R., Silver, J.D., 2007. Hydrogenic Lamb shift in iron Fe^{25+} and fine-structure Lamb shift. *Phys. Rev. A* 76, 042116–1–19.
- Chantler, C.T., Laming, J.M., Silver, J.D., Dietrich, D.D., Mokler, P.H., Finch, E.C., Rosner, S.D., 2009a. Hydrogenic lamb shift in Ge^{31+} and the fine-structure lamb shift. *Phys. Rev. A* 80, 022508.
- Chantler, C.T., Laming, J.M., Silver, J.D., Dietrich, D.D., Mokler, P.H., Finch, E.C., Rosner, S.D., 2009b. The Hydrogenic Lamb Shift in Germanium, Ge^{31+} and fine structure Lamb shift. *Phys. Rev. A* 80, 022508–1–28.
- Chantler, C.T., Lowe, J.A., Grant, I.P., 2010. Multiconfiguration Dirac fock calculations in open shell atoms: Convergence methods and satellite spectra of copper K α photoemission spectrum. *Phys. Rev. A* 82, 052505–1–4.
- Chantler, C.T., Nguyen, T.V.B., Lowe, J.A., Grant, I.P., 2013. Relativistic calculation of transition probabilities for 557.7nm and 297.2nm emission lines in oxygen. *Astrophys. J.* 769 (1), 84.
- Chantler, C.T., Nguyen, T.V.B., Lowe, J.A., Grant, I.P., 2014a. Convergence of the Breit interaction in self-consistent and configuration-interaction approaches. *Phys. Rev. A* 90, 062504. <http://dx.doi.org/10.1103/PhysRevA.90.062504>.
- Chantler, C.T., Paterson, D., Hudson, L.T., Serpa, F.G., Gillaspay, J.D., Takacs, E., 2000. Absolute measurement of the resonance lines in heliumlike vanadium on an electron-beam ion trap. *Phys. Rev. A* 62, 042501–1–13.
- Chantler, C.T., Payne, A.T., Kinnane, M.N., Gillaspay, J.D., Hudson, L.T., Smale, L.F., 2014b. X-ray measurements in helium-like atoms increased discrepancy between experiment and theoretical QED. *New J. Phys.* 16, 123037 – 1 – 15.
- Cocke, C.L., Curmutte, B., Randall, R., 1974. X-ray emission from foil-exited sulphur beams. *Phys. Rev. A* 9, 1823–1827. <http://dx.doi.org/10.1103/PhysRevA91823>.
- Deslattes, R.D., Beyer, H.F., Folkmann, F., 1984. Precision X-ray wavelength measurements in helium-like argon recoil ions. *J. Phys. B* 17, L689–694.
- Deslattes, R.D., Schuch, R., Justiniano, E., 1985. Application of decelerated bare nuclei to precision spectroscopy of one-electron ions. *Phys. Rev. A* 32, 1911–1913.
- Dohmann, H.D., Mann, R., 1979. Measurement of the lifetime of the 3P_2 and $^4P_4/5$ states in Ar^{16+} and Ar^{15+} . *Z. Phys. A Hadrons Nuclei* 291, 15–22, 101007/BF01415809.
- Gaigalas, G., Rudzikas, Z., Gaidamauskas, E., Rynkun, P., Alkauskas, A., 2010. Peculiarities of spectroscopic properties of W^{24+} . *Phys. Rev. A* 82, 014502.
- Gaigalas, G., Rynkun, P., Alkauskas, A., Rudzikas, Z., 2012. The energy levels and radiative transition probabilities for electric quadrupole and magnetic dipole transitions among the levels of the ground configuration, $[Kr]4d^{10}4f^4$, of W^{24+} . *At. Data Nucl. Data Tables* 98 (3), 391–436.
- Grant, I.P., 1974. Gauge invariance and relativistic radiative transitions. *J. Phys. B* 7 (12), 1458.
- Grant, I.P., 1980. Many-Electron Effects in the Theory of Nuclear Volume Isotope Shift. *Phys. Scr.* 21, 443–447.
- Indelicato, P., Boucard, S., Lindroth, E., 1998. Relativistic and many-body effects in K, L, and M shell ionization energy for elements with $10 < Z < 100$ and the determination of the 1s Lamb shift for heavy elements. *Eur. Phys. J. D* 3, 29–41.
- Indelicato, P., Briand, J.-P., Tavernier, M., Liesen, D., 1986. Experimental study of relativistic corrections and QED effects in heliumlike krypton ions. *Z. Phys. D* 2, 249–250.
- Indelicato, P., Mohr, P.J., 2001. Coordinate-space approach to the bound-electron self-energy: Self-energy screening calculation. *Phys. Rev. A* 63, 052507. <http://dx.doi.org/10.1103/PhysRevA.63.052507>.
- Jönsson, P., Gaigalas, G., Bieroń, J., Froese-Fischer, C., Grant, I.P., 2013. New version: Grasp2K relativistic atomic structure package. *Comp. Phys. Commun.* 184 (9), 2197–2203.
- Jönsson, P., He, X., Froese-Fischer, C., Grant, I.P., 2007. The GRASP2K relativistic atomic structure package. *Comput. Phys. Commun.* 177 (7), 597–622.
- Källne, E., Källne, J., Richard, P., Stöckli, M., 1984. Precision measurement of the H-like x-ray spectrum of Cl and the 1s lamb shift. *J. Phys. B* 17, L115–L120.
- Kubicek, K., Braun, J., Bruhns, H., Lopez-Urrutia, J.R.C., Ullrich, J., 2012. High-precision laser-assisted absolute determination of x-ray diffraction angles. *Rev. Sci. Instr.* 83, 013102–1–8.
- Kubicek, K., Bruhns, H., Braun, J., Lopez-Urrutia, J.R.C., Ullrich, J., 2009. Two-loop QED contributions tests with mid-Z He-like ions. *J. Phys. Conf. Ser.* 163 (1), 012007–1–6.
- Laming, J.M., Chantler, C.T., Silver, J.D., Dietrich, D.D., Finch, E.C., Mokler, P.H., Rosner, S.D., 1988. A differential measurement of the ground state lamb shift in hydrogenic Germanium, Ge^{31+} . *NIM B31*, 21–23.
- Le Bigot, É.-O., Indelicato, P., Mohr, P., 2001. QED self-energy contribution to highly excited atomic states. *Phys. Rev. A* 64, 052508.
- Li, M.C., Si, R., Brage, T., Hutton, R., Zou, Y.M., 2018. Proposal of highly accurate tests of Breit and QED effects in the ground state $2p^5$ of the F-like isoelectronic sequence. *Phys. Rev. A* 98, 020502.
- Lowe, J.A., Chantler, C.T., Grant, I.P., 2013. Self-energy screening approximations in multi-electron atoms. *Radiat. Phys. Chem.* 85, 118–123.
- Lu, Q., Yan, C.L., Xu, G.Q., Fu, N., Yang, Y., Zou, Y., Volotka, A.V., Xiao, J., Nakamura, N., Hutton, R., 2020. Direct measurements for the fine-structure splitting of S viii and Cl ix. *Phys. Rev. A* 102, 042817.
- MacLaren, S., Beiersdorfer, P., Vogel, D.A., Knapp, D., Marrs, R.E., Wong, K., Zasadzinski, R., 1992. Precision measurement of the $K\alpha$ transitions in heliumlike Ge^{30+} . *Phys. Rev. A* 45, 329–332. <http://dx.doi.org/10.1103/PhysRevA45329>.
- Marmar, E., Rice, J., Källne, E., Källne, J., LaVilla, R., 1986. Precision measurement of the 1s lamb shift in hydrogen like argon. *Phys. Rev. A* 33, 774–777.
- Mohr, P.J., 1974. Self-Energy Radiative Corrections in Hydrogen-Like Systems. *Ann. Physics* 88, 26–51.
- Mohr, P.J., 1983. Energy Levels of Hydrogen-Like Atoms Predicted By Quantum Electrodynamics, $10 \leq Z \leq 40$. *At. Data Nucl. Data Tables* 29 (3), 453–466.
- Mohr, P.J., Kim, Y.K., 1992. Self-energy of excited states in a strong Coulomb field. *Phys. Rev. A* 45 (5), 2727–2735.
- Nazé, C., Gaidamauskas, E., Gaigalas, G., Godefroid, M., Jönsson, P., 2013. ris3: A program for relativistic isotope shift calculations. *Comput. Phys. Comm.* 184 (9), 2187–2196.
- Neupert, W.M., 1971. Satellite lines in the solar X-ray spectrum. *Sol. Phys.* 18, 474–488, 101007/BF00149069.
- Nguyen, T.V.B., Melia, H.A., Janssens, F.I., Chantler, C.T., 2022a. Multiconfiguration Dirac-Hartree-Fock theory for copper $K\alpha$ and $K\beta$ diagram lines, satellite spectra, and *ab initio* determination of single and double shake probabilities. *Phys. Rev. A* 105, 022811. <http://dx.doi.org/10.1103/PhysRevA.105.022811>, URL: <https://link.aps.org/doi/10.1103/PhysRevA.105.022811>.
- Nguyen, T., Melia, H., Janssens, F., Chantler, C., 2022b. Theory of copper $K\alpha$ and $K\beta$ diagram lines, satellite spectra, and *ab initio* determination of single and double shake probabilities. *Phys. Lett. A* 426, 127900. <http://dx.doi.org/10.1016/j.physleta.2021.127900>, URL: <https://www.sciencedirect.com/science/article/pii/S0375960121007659>.
- Parpia, F.A., Froese-Fischer, C., Grant, I.P., 1996. GRASP92: A package for large-scale relativistic atomic structure calculations. *Comput. Phys. Comm.* 94 (2–3), 249–271.
- Payne, A.T., Chantler, C.T., Kinnane, M.N., Gillaspay, J.D., Hudson, L.T., Smale, L.F., 2014. Helium-like titanium X-ray spectrum as a probe of QED computation. *J. Phys. B* 47, 185001–1–8.
- Richard, P., Stockli, M., Deslattes, R.D., Cowan, P., LaVilla, R.E., Johnson, B., Jones, K., Meron, M., Mann, R., Scharfner, K., 1984. Measurement of the 1s lamb shift in hydrogenlike chlorine. *Phys. Rev. A* 29, 2939–2942.
- Rzadkiewicz, J., Yang, Y., Koziol, K., O'Mullane, M.G., Patel, A., Xiao, J., Yao, K., Shen, Y., Lu, D., Hutton, R., Zou, Y., Contributors, J., 2018. High-resolution tungsten spectroscopy relevant to the diagnostic of high-temperature tokamak plasmas. *Phys. Rev. A* 97, 052501.
- Schleinkofer, L., Bell, F., Betz, H.-D., Trollman, G., Rothermel, J., 1982. Precision Wavelength Determination of $2^1P_1-1^1S_0$ and $2^3P_1-1^1S_0$ Transitions in Helium-Like Sulfur Ions. *Phys. Scripta* 25, 917–923.
- Scofield, J.H., 1973. Theoretical photoionization cross sections from 1 keV to 1500 keV. LLNL Report. UCRI–51326.
- Shabaev, V.M., Tupitsyn, I.I., Kaygorodov, M.Y., Kozhedub, Y.S., Malyshev, A.V., Mironova, D.V., 2020. QED corrections to the $^2P_{1/2}-^2P_{3/2}$ fine structure in fluorinelike ions: Model lamb-shift-operator approach. *Phys. Rev. A* 101, 052502.
- Shabaev, V.M., Tupitsyn, I.I., Yerokhin, V.A., 2013. Model operator approach to the lamb shift calculations in relativistic many-electron atoms. *Phys. Rev. A* 88, 012513.
- Shabaev, V., Tupitsyn, I., Yerokhin, V., 2015. QEDMOD: Fortran program for calculating the model lamb-shift operator. *Comput. Phys. Comm.* 189, 175–181.
- Si, R., Guo, X.L., Brage, T., Chen, C.Y., Hutton, R., Fischer, C.F., 2018. Breit and QED effects on the $3d^9\ ^2D_{3/2} \rightarrow ^2D_{5/2}$ transition energy in Co-like ions. *Phys. Rev. A* 98, 012504.
- Silver, J., McClelland, A., Laming, J., Rosner, S., Chandler, G., Dietrich, D., Egan, P., 1987. Simultaneous observation of Lyman- α and Balmer- β transitions in hydrogenic iron, Fe^{25+} : A novel technique for 1s lamb-shift measurement. *Phys. Rev. A* 36, 1515–1518.
- Thorn, D.B., Gu, M.F., Brown, G.V., Beiersdorfer, P., Porter, F.S., Kilbourne, C.A., Kelley, R.L., 2009. Precision measurement of the K-shell spectrum from highly charged xenon with an array of X-Ray calorimeters. *Phys. Rev. Lett.* 103, 163001–1–4.
- Volotka, A.V., Bilal, M., Beerwerth, R., Ma, X., Stöhlker, T., Fritzsche, S., 2019. QED radiative corrections to the $^2P_{1/2}-^2P_{3/2}$ fine structure in fluorinelike ions. *Phys. Rev. A* 100, 010502.
- Welton, T.A., 1948. Some observable effects of the quantum-mechanical fluctuations of the electromagnetic field. *Phys. Rev.* 74, 1157–1167.
- Widmann, K., Beiersdorfer, P., Decaux, V., 1995. Wavelength measurements of the He-like krypton K-shell spectrum. *Nucl. Instrum. Methods B* 98, 45–47.
- Widmann, K., Beiersdorfer, P., Decaux, V., Bitter, M., 1996. Measurements of the K α transition energies of heliumlike krypton. *Phys. Rev. A* 53, 2200–2205. <http://dx.doi.org/10.1103/PhysRevA532200>.
- Yerokhin, V.A., Artemyev, A.N., Shabaev, V.M., 1997. Two-electron self-energy contribution to the ground-state energy of helium-like ions. *Phys. Lett. A* 234 (5), 361–366.

Yerokhin, V.A., Shabaev, V.M., 1995. Accurate calculation of self-energy screening diagrams for high Z helium-like atoms. *Phys. Lett. A* 207 (5), 274–280.

Zatsarinny, O., Froese Fischer, C., 2016. DBSR_HF: A B-spline Dirac-Hartree-Fock program. *Comput. Phys. Comm.* 202, 287–303.

Zhang, C.Y., Wang, K., Godefroid, M., Jönsson, P., Si, R., Chen, C.Y., 2020. Benchmarking calculations with spectroscopic accuracy of excitation energies and wavelengths in sulfur-like tungsten. *Phys. Rev. A* 101, 032509.